

# Viscous lock-exchange in rectangular channels

J. MARTIN, N. RAKOTOMALALA, L. TALON  
AND D. SALIN†

Université Pierre et Marie Curie, Université Paris-Sud, CNRS, Laboratoire FAST,  
Bâtiment 502, Rue du Belvedere, Campus Universitaire,  
F-91405 Orsay CEDEX, France

(Received 24 March 2010; revised 23 September 2010; accepted 30 November 2010;  
first published online 14 February 2011)

In a viscous lock-exchange gravity current, which describes the reciprocal exchange of two fluids of different densities in a horizontal channel, the front between two Newtonian fluids spreads as the square root of time. The resulting diffusion coefficient reflects the competition between the buoyancy-driving effect and the viscous damping, and depends on the geometry of the channel. This lock-exchange diffusion coefficient has already been computed for a porous medium, a two-dimensional (2D) Stokes flow between two parallel horizontal boundaries separated by a vertical height  $H$  and, recently, for a cylindrical tube. In the present paper, we calculate it, analytically, for a rectangular channel (horizontal thickness  $b$  and vertical height  $H$ ) of any aspect ratio ( $H/b$ ) and compare our results with experiments in horizontal rectangular channels for a wide range of aspect ratios (1/10 to 10). We also discuss the 2D Stokes–Darcy model for flows in Hele–Shaw cells and show that it leads to a rather good approximation, when an appropriate Brinkman correction is used.

**Key words:** gravity currents

---

## 1. Introduction

The lock-exchange configuration refers to the release, under gravity, of the interface between two fluids of different densities, confined in the section of a horizontal channel. This physical process has prompted renewed interest, as a part of the carbon dioxide sequestration issues (Neufeld & Huppert 2009). Figure 1(*a*) shows the initial lock-exchange situation of a so-called full-depth release. The two fluids, initially separated by a vertical barrier (the lock gate), fill the whole section of the tank. When the gate is withdrawn (figure 1*b*), buoyancy drives the denser fluid along the bottom wall, while the lighter fluid flows in the opposite direction at the top of the channel. The so-called lock-exchange results in the elongation of the interface between the two fluids along the horizontal direction. Different regimes have been reported for the velocity and shape of the elongating interface. The slumping phase refers to the initial regime where inertia dominates over viscous forces, which typically applies for the case of salted and fresh water in a tank. In this regime, Benjamin (1968) and, more recently, Shin, Dalziel & Linden (2004) have shown that in the presence of a small density contrast (i.e. in the Boussinesq approximation  $\Delta\rho \ll \rho$ ), the two opposite currents travelled at the same constant velocity. When the Boussinesq

† Email address for correspondence: [salin@fast.u-psud.fr](mailto:salin@fast.u-psud.fr)

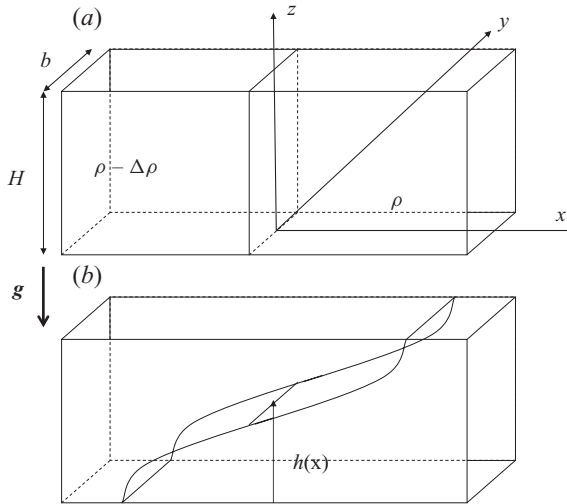


FIGURE 1. Sketch of the rectangular cell of height  $H$  in the gravity direction and width  $b$ . (a) Initial configuration where the heavy fluid of density,  $\rho$ , is separated from the light fluid of density,  $\rho - \Delta\rho$ , by a vertical gate (the  $y$ - $z$  plane). (b) After removing the gate, buoyancy differences cause the denser fluid to flow in one direction along the bottom of the vessel, while the lighter fluid flows in the opposite direction at the top of the vessel. The goal is to determine the space and time dependencies of the pseudo-interface,  $h(x, t)$ .

approximation does not apply, Lowe, Rottman & Linden (2005), Birman, Martin & Meiburg (2005), Cantero *et al.* (2007) and Bonometti, Balachandar & Magnaudet (2008) showed that the two opposite fronts did travel at constant, but with different velocities. However, this interface elongation, proportional to the time, is slowed down at later stages, in the viscous phase, where dissipation prevails over inertia. In the latter regime, the interface elongates as  $t^\alpha$ , where the exponent  $\alpha$ , smaller than unity, may take different values depending on the geometry and the confinement of the flow (Didden & Maxworthy 1982; Huppert 1982; Gratton & Minotti 1990; Cantero *et al.* 2007; Takagi & Huppert 2007; Hallez & Magnaudet 2009). In porous media, Bear (1988) and Huppert & Woods (1995) predicted an interface spreading proportionally to the square root of time that Séon *et al.* (2007) observed in a horizontal cylindrical tube. Such a spreading can be quantified with a diffusion coefficient, which reflects the balance between the buoyancy driving and the viscous damping. This coefficient, which depends on the nature and the geometry of the flow, has been computed for a porous medium by Huppert & Woods (1995), for a two-dimensional (2D) Stokes flow between two parallel horizontal boundaries separated by a vertical height  $H$  by E. Hinch (2007, personal communication) and Taghavi *et al.* (2009), and for a cylindrical tube by Séon *et al.* (2007). However, to our knowledge, such a diffusion coefficient has not been derived for a rectangular channel (horizontal thickness  $b$  and vertical height  $H$ , figure 1), for which one expects to recover the porous medium regime for  $b \ll H$ , and, possibly, the Stokes flow regime for  $b \gg H$ . In order to gather the limiting cases in the same paper, we first recall the results for porous media and 2D Stokes flows, together with the tube case, for the sake of comparison. Then we compute, for a rectangular channel of aspect ratio,  $H/b$ , the dependence of the interface  $h(x, t)$  and the corresponding viscous lock-exchange diffusion coefficient. We also test the so-called Stokes–Darcy 2D model against this lock-exchange configuration. Finally,

we test and validate our theoretical results with experiments in horizontal rectangular channels for a wide range of aspect ratios (1/10 to 10).

## 2. Lock-exchange in different geometries

Let us first recall the basic hypotheses on the viscous gravity currents, common to the different geometries, used for instance by Huppert & Woods (1995) or E. Hinch (2007, personal communication). As sketched in figure 1, the interface between the two fluids is assumed independent on the  $y$ -direction. Its distance from the bottom boundary of the vessel is denoted by  $h(x, t)$ . This interface can be a pseudo-interface between two miscible fluids for which molecular diffusion can be neglected or between two immiscible fluids, provided that the interfacial tension can be neglected. The flow is assumed to be quasi-parallel to the horizontal  $x$  axis. This is a key hypothesis. Neglecting accordingly the vertical component of the fluid velocity implies that the vertical pressure gradient follows the hydrostatic variations:  $\partial p / \partial z = -\rho g$ . This hypothesis is violated at short times, immediately after the opening of the gate, but should become valid at later stages, as soon as the interface has slumped over a distance larger than  $H$ , thus ensuring a small enough local slope  $\partial h / \partial x$ . Then, the pressures  $P_+$  and  $P_-$  in both the lower,  $0 < z < h(x, t)$ , and upper layers,  $h(x, t) < z < H$ , respectively, are written as

$$P_+ = p(x, t) - \rho_+ g z, \quad P_- = P_+ + \Delta \rho g (z - h(x, t)), \quad (2.1)$$

where  $p(x, t)$  denotes the pressure at the lower wall,  $z = 0$ . The difference between the horizontal pressure gradients in the two fluids is therefore linked to the interface slope by

$$\frac{\partial P_+}{\partial x} - \frac{\partial P_-}{\partial x} = \Delta \rho g \frac{\partial h}{\partial x}. \quad (2.2)$$

The time evolution of the interface,  $h(x, t)$ , is governed by the mass conservation of each fluid (see figure 1 for notations). For instance, for the heavier bottom layer we have

$$\frac{\partial h}{\partial t} + \frac{\partial q}{\partial x} = 0, \quad (2.3)$$

where  $q(x, t) = q_+(x, t)$  is the horizontal flux ( $\text{m}^2 \text{s}^{-1}$ ) of the denser fluid at the location  $x$ :

$$q(x, t) = q_+(x, t) = \int_0^h \frac{1}{b} \int u_x(x, y, z, t) dy dz, \quad (2.4)$$

with  $u_x(x, y, z, t)$  being the  $x$ -velocity component and  $b$  being the spanwise length (the  $y$  integration is along this spanwise length). Moreover, in our configuration of uniform section along the horizontal axis  $x$ ,  $u_x(x, y, z, t)$  must also satisfy the no-net-flux condition

$$q_+(x, t) + q_-(x, t) = \int_0^H \frac{1}{b} \int u_x(x, y, z, t) dy dz = 0. \quad (2.5)$$

We will see in the following that in the viscous regime of interest, the horizontal velocity component  $u_x$ , solution of either a Darcy or a Stokes equation, is proportional to the pressure gradient in each fluid layer. Such solutions combined with (2.2), (2.4) and (2.5) allow to eliminate the pressure gradients and derive an expression of the

flux  $q$ , of the form

$$q = -Df \left( \frac{h}{H} \right) \frac{\partial h}{\partial x}, \quad (2.6)$$

where  $D$  is written as

$$D = \tau \frac{\Delta \rho g}{\eta}, \quad (2.7)$$

and the constant  $\tau$  (scaling with a volume) and the function  $f$  depend on the geometry and the flow equation, and  $\eta$  is the dynamic viscosity. Using the expression (2.6) for the flux, (2.3) admits a self-similar solution  $h(\zeta) = H \psi(\zeta)$ , with the similarity variable  $\zeta = x/\sqrt{Dt}$ , which obeys

$$-\zeta \frac{d\psi}{d\zeta} = 2 \frac{d}{d\zeta} \left( f(\psi) \frac{d\psi}{d\zeta} \right). \quad (2.8)$$

This equation may alternatively be rewritten, in terms of  $\zeta(\psi)$ , as

$$\zeta \left( \frac{d\zeta}{d\psi} \right)^2 - 2f \frac{d^2\zeta}{d\psi^2} + 2 \frac{df}{d\psi} \left( \frac{d\zeta}{d\psi} \right) = 0. \quad (2.9)$$

The solution of the above equations can be found analytically or numerically, depending on the complexity of the normalized flux function  $f(\psi)$ . In the following, we first recall the case of porous media treated by Huppert & Woods (1995) and the 2D Stokes flow addressed by E. Hinch (2007, personal communication) and Taghavi *et al.* (2009). We note that Taghavi *et al.* (2009) included the effects of the rheological properties of the fluids. However, in order to focus on the geometrical aspects, here we assume that both fluids are Newtonian and have the same viscosity.

### 2.1. Lock-exchange in porous media

For a homogeneous layer of porous medium of permeability  $\kappa$  (see for instance Huppert & Woods 1995), the flow in each fluid is given by Darcy's law, which relates the velocity in each phase to the local pressure gradient,

$$u_{x\pm} = -\frac{\kappa}{\eta} \frac{\partial P_{\pm}}{\partial x} \quad (2.10)$$

At a given location  $x$ , the velocity is uniform in each layer and the no-net-flux condition (see (2.5)) is simply written as  $hu_{x+} + (H-h)u_{x-} = 0$ . This condition combined with (2.10) and (2.2) leads to (2.6), and thus (combined with (2.3)) to (2.8) with a diffusion coefficient and a flux function:

$$D_{PM} = \kappa H \frac{\Delta \rho g}{\eta}, \quad (2.11)$$

$$f_{PM}(\psi) = \psi(1-\psi). \quad (2.12)$$

The solution of (2.8) in the similarity variable  $\zeta = x/\sqrt{D_{PM}t}$  is then a linear profile (Huppert & Woods 1995):

$$\psi = h(x, t)/H = (1 + \zeta)/2. \quad (2.13)$$

The so-obtained front profile in homogeneous porous media is displayed in figure 2 (straight line) together with those for rectangular cells (referred to in §2.3). The leading ( $\psi = 0$ ,  $\zeta = -1$ ) and trailing ( $\psi = 1$ ,  $\zeta = 1$ ) edges spread as  $\sqrt{D_{PM}t}$ . Therefore, the lock-exchange diffusion coefficient for porous media is  $D_{PM}$ . Note that Bear (1988) reported a numerical integration of (2.8), indicating that the gravity current

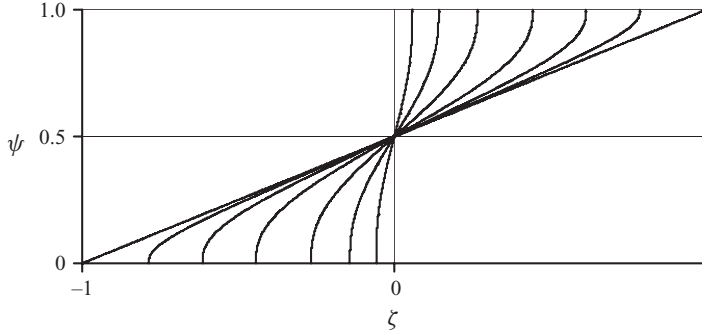


FIGURE 2. Lock-exchange interface  $\psi(\zeta)$  between the two fluids for rectangular cells of different aspect ratios  $\Gamma = H/b$ . The straight line of slope 0.5 corresponds to the Darcy porous media limit (2.13). The other curves correspond to the case of a rectangular cross-section channel (§ 2.3). From the bottom left to right,  $\Gamma = 10, 4, 2, 1, 0.5$  and  $0.2$ .

spreads as the square root of time. Note that the corresponding result for a Hele-Shaw cell, which is two parallel plates of height,  $H$ , separated by a tiny gap  $b$  ( $b \ll H$ ), is obtained using the permeability  $\kappa = b^2/12$ :

$$D_{HS} = \frac{b^2 H \Delta \rho g}{12 \eta}. \quad (2.14)$$

## 2.2. Lock-exchange for a 2D Stokes flow between two horizontal boundaries

For a 2D Stokes flow between two horizontal parallel boundaries, separated by a height  $H$  in the plane ( $z$ - $x$ ) (assuming invariance along the  $y$ -direction), the flow in each fluid is given by the Stokes equation:

$$\eta \nabla^2 u_{x\pm}(x, z) = \frac{\partial P_{\pm}}{\partial x}. \quad (2.15)$$

At a given location  $x$ , the velocity profile consists of two parabola profiles matching the no-slip boundary conditions at the bottom and top boundaries ( $u_{x+}(x, 0) = u_{x-}(x, H) = 0$ ) and the continuity of the velocity ( $u_{x-}(x, h) = u_{x+}(x, h)$ ) and the shear stress ( $\eta \partial u_{x-}(x, h)/\partial z = \eta \partial u_{x+}(x, h)/\partial z$ ) at the interface,  $z = h$ .

Using the no-net-flux condition (see (2.5)) and (2.2), we obtain (2.6), which enables us to rewrite (2.3), in the form of (2.8) or (2.9), as

$$D = \frac{H^3 \Delta \rho g}{3 \eta}, \quad (2.16)$$

$$f(\psi) = \psi^3(1 - \psi)^3. \quad (2.17)$$

Note that the polynomial development of the solution of (2.9) around  $\psi = 0$  gives  $\zeta = -\zeta_0 + 2\psi^3/(3\zeta_0)$ . Thus, the location  $\zeta(\psi = 0) = -\zeta_0$  of the leading edge of the interface is indeed constant in the similarity variable. Moreover, the development shows that the slope of the interface is vertical at the bottom wall ( $\psi = 0$ ). This is also the case at the upper wall ( $\psi = 1$ ), as the problem is symmetric with respect to the centre of the cell. We note that in the presence of such a vertical slope, our (horizontal) quasi-parallel flow assumption falls locally, but it is still valid upstream and downstream, where the slope of the interface remains small. The solution of (2.9) can be found numerically using a shooting method similar to that used by E.

Hinch (2007, personal communication) and Taghavi *et al.* (2009). It was computed starting the integration of (2.9) from  $(\psi = 0.5, \zeta = 0)$  and matching the asymptotic development in the vicinity of  $\psi = 0$ . From the so-obtained solution, one can deduce the spreading diffusion coefficient between the leading edge ( $h = 0, -\zeta_0 = -0.1607$ ) and the trailing edge ( $h = H, \zeta_0$ ) of the front, from  $[0.5(x(h = 0) - x(h = H))]^2 = Dt$ , which gives  $D_{2D} = D \zeta_0^2$ , so that

$$D_{2D} = 0.0086 H^3 \frac{\Delta \rho g}{\eta}. \quad (2.18)$$

This result is in agreement with that found by E. Hinch (2007, personal communication). Taghavi *et al.* (2009) provided five  $\psi(\zeta)$  plots in their figure 9, corresponding to different viscosity ratios including our case. From that figure, we may obtain a value of their similarity variable,  $\eta_0 \sim 0.09$ , which is consistent with our finding  $\zeta_0 = 0.1607$ , when taking into account their definition of the similarity variable,  $\zeta = \eta \sqrt{3}$ .

For completeness,  $D_{2D}$  may be compared with the result for a cylindrical tube of diameter  $d$  (Séon *et al.* 2007):

$$D_T = 0.0054 d^3 \frac{\Delta \rho g}{\eta}. \quad (2.19)$$

The above expression is indeed very close to the 2D result, with  $d$  playing the role of  $H$ .

### 2.3. Lock-exchange in a rectangular cross-section channel

This article aims to extend the computation of the lock-exchange diffusion coefficient to rectangular cells of arbitrary cross-sections  $H \times b$  (see figure 1). In the following, the cross-sectional aspect ratio will be denoted by  $\Gamma = H/b$ . As in the previous section, a quasi-parallel flow approximation is assumed (i.e. small interface slope), which leads to (2.2) for the pressure gradient. We will also assume the invariance of the interface location along the gap direction  $y$ . This requires that the deformation of the interface, induced by the flow profile along the direction  $y$ , relaxes much more quickly than the gradient along  $x$ . The flow in each fluid obeys a 3D Stokes equation:

$$\eta \nabla^2 u_{x\pm}(x, y, z) = \frac{\partial P_{\pm}}{\partial x}. \quad (2.20)$$

In order to solve this equation, we follow the series decomposition in Fourier modes of the velocity field used by Gondret *et al.* (1997), who addressed the issue of the parallel flow of two fluids of different viscosities in a rectangular cell. This issue is very close to ours, as it requires to solve the Poisson equation (2.20), but with different viscosities and the same pressure gradient for both fluids in Gondret *et al.* (1997). The method used was to split the velocity into two terms,  $u_{x\pm}(x, y, z) = u_{x\pm}^*(x, y) + u_{x\pm}^{**}(x, y, z)$ . Here, the first term

$$u_{x\pm}^*(x, y) = \frac{b^2}{8\eta} \frac{\partial P_{\pm}}{\partial x} \left[ 1 - \left( \frac{2y}{b} \right)^2 \right] \quad (2.21)$$

is the Poiseuille-like unperturbed velocity far away from the interface. The second term satisfies the Laplace equation,  $\nabla^2 u_{x\pm}^{**}(x, y, z) = 0$ , and vanishes far away from the interface. Its expression in terms of a sum of Fourier modes leads to a velocity

profile of the form

$$u_{x\pm}(x, y, z) = \frac{b^2}{8\eta} \frac{\partial P_{\pm}}{\partial x} \left\{ 1 - \left( \frac{2y}{b} \right)^2 + \sum_{n=1}^{\infty} \frac{32(-1)^n (a_{\pm n} e^{(2n-1)\frac{\pi(z-H/2)}{b}} + b_{\pm n} e^{-(2n-1)\frac{\pi(z-H/2)}{b}})}{(2n-1)^3 \pi^3} \cos \left[ (2n-1) \frac{\pi y}{b} \right] \right\}, \quad (2.22)$$

in which the no-slip boundary conditions at the two vertical walls ( $u_{x\pm}(x, y = \pm b/2, z) = 0$ ) have been taken into account. Each Fourier mode ( $(2n-1)\pi/b$ ) involves two constants for each fluid,  $a_{\pm n}$  and  $b_{\pm n}$ . These four constants are determined by using the no-slip boundary conditions at the bottom and top of the cell ( $u_{x+}(x, y, z=0) = u_{x-}(x, y, z=H) = 0$ ) and the continuity of the velocity ( $u_{x+}(x, y, z=h) = u_{x-}(x, y, z=h)$ ) and the shear stress ( $\eta \partial u_{x+}(x, y, z=h)/\partial z = \eta \partial u_{x-}(x, y, z=h)/\partial z$ ) at the interface. Combining the so-obtained expressions for the velocity with (2.2) and the no-net-flux condition (2.5), one obtains the horizontal flux of the heavy fluid (2.6):

$$q = -D_{HS} f_{\Gamma}(h/H) \frac{\partial h}{\partial x}, \quad (2.23)$$

with

$$D_{HS} = \frac{b^2 H \Delta \rho g}{12\eta}, \quad (2.24)$$

$$f_{\Gamma}(\psi) = \frac{\psi + \alpha_{\Gamma}(\psi)}{1 - \gamma_{\Gamma}} (1 - \psi - \alpha_{\Gamma}(\psi) - \gamma_{\Gamma}) - \delta_{\Gamma}(\psi), \quad (2.25)$$

where

$$\alpha_{\Gamma}(\psi) = \frac{1}{\Gamma} \sum_{n=1}^{\infty} \frac{96 (1 + e^{\Gamma(1-\psi)(2n-1)\pi}) (1 - e^{\Gamma\psi(2n-1)\pi})}{(1 + e^{\Gamma(2n-1)\pi}) (2n-1)^5 \pi^5}, \quad (2.26)$$

$$\delta_{\Gamma}(\psi) = \frac{1}{\Gamma} \sum_{n=1}^{\infty} \frac{48 (1 - e^{\Gamma(1-\psi)(2n-1)\pi})^2 (1 - e^{\Gamma\psi(2n-1)\pi})^2}{(-1 + e^{2\Gamma(2n-1)\pi}) (2n-1)^5 \pi^5}, \quad (2.27)$$

$$\gamma_{\Gamma} = \frac{1}{\Gamma} \sum_{n=1}^{\infty} \frac{192 \tanh \left( \frac{\Gamma(2n-1)\pi}{2} \right)}{(2n-1)^5 \pi^5}. \quad (2.28)$$

Equation (2.23) admits a self-similar solution,  $h(\zeta) = H\psi(\zeta)$ , with the similarity variable  $\zeta = x/\sqrt{D_{HS}t}$ , which obeys (2.8) or (2.9). As previously, it is easier to compute the solution  $\zeta(\psi)$  of (2.9) subject to the corresponding asymptotics,  $\zeta = -\zeta_0 + 8\Gamma^2\psi^3/(3\zeta_0)$  in the vicinity of the boundary,  $\psi = 0$ . We solve this equation using the shooting method previously described and using Mathematica Software. The solutions  $h(\zeta)$  are plotted in figure 2 for different values of the cell aspect ratio  $\Gamma$ . We note that in contrast with Darcy predictions (straight line in figure 2), but similar to the case of the 2D Stokes flow, the profiles  $h(\zeta)$  exhibit vertical slopes at the edges of the cell. We note also that such vertical slopes were observed in the experiments by Séon *et al.* (2007) and Huppert & Woods (1995). When comparing their experiments in a Hele-Shaw cell with Darcy predictions, Huppert & Woods (1995) reported that ‘[s]ome discrepancies develop near the leading edge of the current as a result of the increasing importance of the bottom friction at the nose’ (figure 2 of Huppert &

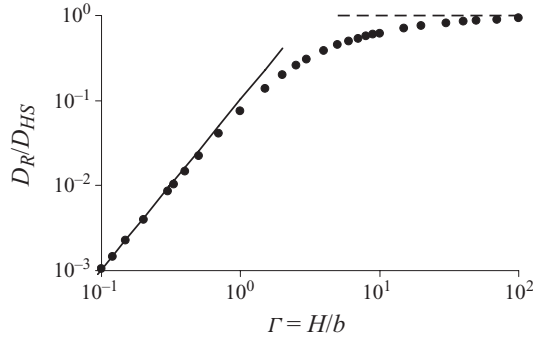


FIGURE 3. Log–log plot of the normalized lock-exchange diffusion coefficient,  $D_R/D_{HS}$ , versus the aspect ratio  $\Gamma = H/b$ , for rectangular cells.  $D_R$  is normalized by the diffusion coefficient  $D_{HS} = b^2 H \Delta \rho g / (12 \eta)$  (see (2.14)), obtained for the Hele-Shaw cell limit, also corresponding to a 2D porous medium. Accordingly, the latter regime corresponds to the dashed line ( $D_R/D_{HS} = 1$ ) in this representation. The solid line corresponds to the 2D Stokes limit (2.18), leading to a slope 2 in this representation.

Woods 1995). This mismatch will be addressed in the next section. According to the so-obtained profiles, stationary in the similarity variable  $\zeta$ , the leading and trailing edges of the front spread as the square root of time, and a lock-exchange diffusion coefficient, dependent on the cell aspect ratio, can be defined:

$$D_R = \frac{b^2 H \Delta \rho g}{12 \eta} F\left(\frac{H}{b}\right) = D_{HS} F\left(\frac{H}{b}\right). \quad (2.29)$$

Figure 3 displays a log–log plot of the normalized rectangular cell lock-exchange diffusion coefficient,  $D_R/D_{HS} = F(H/b)$ , versus the aspect ratio  $\Gamma = H/b$ . At small aspect ratios,  $\Gamma < 1$ , the diffusion coefficient falls on top of the full line of slope 2, which corresponds to the 2D Stokes flow between boundaries distant of  $H$  ( $b \rightarrow \infty$ , see (2.18)). At large aspect ratios,  $\Gamma \rightarrow 100$ , the diffusion coefficient approaches the dashed line,  $D_R/D_{HS} = 1$ , obtained for the case of 2D homogeneous porous medium (2.14). We note that the latter case, which corresponds to a Hele-Shaw cell of infinite aspect ratio, overestimates the lock-exchange diffusion coefficient by a relative amount of about 30 % for aspect ratios as large as  $\Gamma = 10$ –20.

### 3. Two-dimensional Stokes–Darcy model for lock-exchange in a rectangular cross-section channel

The above-mentioned failures of the 2D Darcy model at finite aspect ratios may come from the velocity slip condition at the bottom and top edges of the cell ( $z = 0$  and  $z = H$ , respectively). This non-physical condition is indeed required by the use of Darcy equation for the flow, which neglects the momentum diffusion in the presence of velocity gradients, in the plane of the cell ( $z$ – $x$  plane). The momentum diffusion may, however, be taken into account in two dimensions through the so-called Stokes–Darcy equation (see Bizon *et al.* 1997; Ruyer-Quil 2001; Martin, Rakotomalala & Salin 2002a; Zeng, Yortsos & Salin 2003), which is similar to the Darcy–Brinkman equation used in porous media (see Brinkman 1947). This 2D model enables one to handle discontinuities such as cell edges, gap heterogeneities and fluid interfaces (Ruyer-Quil 2001; Martin *et al.* 2002a; Talon *et al.* 2003; Zeng *et al.* 2003) and was successfully applied in the study of Rayleigh–Taylor instability (Fernandez *et al.* 2002; Graf,



Meiburg & Härtel 2002; Martin *et al.* 2002a), dispersion in heterogeneous fractures (Talon *et al.* 2003) and chemical reaction fronts (Martin *et al.* 2002b). Although our present case of interest can be handled with 3D Stokes calculations, it is of interest to test the applicability of the 2D Stokes–Darcy model to the case of deep and narrow cells. Indeed, such a 2D model, once validated, could be a useful tool to address the issue of more complicated cases, such as gravity currents in the presence of viscosity contrasts or in fractures with aperture heterogeneities.

In this model, the flow in the rectangular cell (figure 1) is assumed to be parallel to the plates ( $\mathbf{u}(x, y, z) = (u_x(x, y, z), 0, u_z(x, y, z))$ ) with a Poiseuille parabolic profile across the gap (the key assumption). Using the Stokes equation with this  $y$ -dependency, the gap-averaged fluid velocity  $\mathbf{U}(x, z) = (1/b) \int_{-b/2}^{b/2} \mathbf{u}(x, y, z) dy$  follows a Stokes–Darcy equation, which for the horizontal component of the velocity reads as

$$-\frac{12\eta}{b^2} U_{x\pm}(x, z) + \beta\eta\nabla^2 U_{x\pm}(x, z) = \frac{\partial P_{\pm}}{\partial x}. \quad (3.1)$$

The first term on the left-hand side of (3.1) and the pressure gradient correspond to the Darcy’s law (2.10) with a permeability  $\kappa = b^2/12$  for the Hele-Shaw cell as mentioned above (2.14). The second term on the left-hand side of (3.1) is the Brinkman correction to the Darcy equation (see Brinkman 1947), which involves an effective viscosity  $\beta\eta$ . This effective viscosity may be taken equal to that of the fluid ( $\beta = 1$ ) for the sake of simplicity (or to enable the matching with a 2D Stokes regime at  $\Gamma \rightarrow 0$ ). However, Zeng *et al.* (2003) showed that in the Hele-Shaw cell regime (at large  $\Gamma$ ), the effective viscosity was slightly higher, with  $\beta = 12/\pi^2 \simeq 1.215$ . At a given location  $x$ , integrating (3.1) leads to the two velocity profiles matching the no-slip boundary conditions at the bottom and top boundaries ( $u_{x+}(x, 0) = u_{x-}(x, H) = 0$ ), and the continuity of the velocity ( $u_{x-}(x, h) = u_{x+}(x, h)$ ) and the shear stress ( $\beta\eta \partial u_{x-}(x, h)/\partial z = \beta\eta \partial u_{x+}(x, h)/\partial z$ ) at the interface. Using the no-net-flux condition,  $\int_0^h u_{x+} dz + \int_h^H u_{x-} dz = 0$ , and (2.2), we obtain the horizontal flux (2.4):

$$q(x) = -D_{HS} f_{SD}(h/H) \frac{\partial h}{\partial x}, \quad (3.2)$$

where  $D_{HS}$  is given in (2.14) and the reduced flux function is equal to

$$f_{SD}(\psi) = \frac{1}{4d(d - \tanh d)} \left\{ 2 + 4d^2(1 - \psi)\psi - d \frac{3 \cosh(2d) + \cosh(2d(1 - 2\psi))}{\sinh(2d)} \right. \\ \left. + 4d \frac{(1 - \psi) \cosh(2d(1 - \psi)) + \psi \cosh(2d\psi)}{\sinh(2d)} - 2 \frac{\cosh(d(1 - 2\psi))}{\cosh(d)} \right\}, \quad (3.3)$$

where

$$d = \sqrt{\frac{H^2}{4\kappa\beta}} = \sqrt{\frac{3}{\beta}} \Gamma \quad (3.4)$$

and  $\kappa = b^2/12$ . A comparison of the full 3D calculations for a rectangular channel of aspect ratio  $\Gamma = H/b$  with the 2D approximation can be performed on the flux functions  $f_r(\psi)$  (see (2.25)) and  $f_{SD}(\psi)$  (see (3.3)). These two flux functions are close to each other, within a few per cents. In order to address the comparison in the range of interest for the Hele-Shaw assumption, i.e.  $\Gamma \gg 1$ , we analyse the limit  $\Gamma \rightarrow \infty$

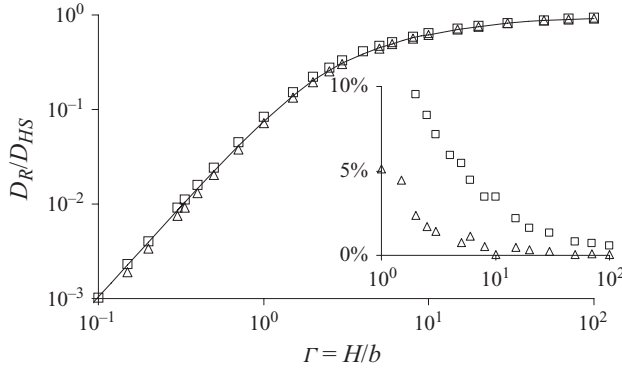


FIGURE 4. Log-log plot of the normalized lock-exchange diffusion coefficient, versus the aspect ratio  $\Gamma = H/b$ , for rectangular cells. The data points, obtained using the 2D Stokes–Darcy model (see (4)) with Brinkman viscosity factors  $\beta = 1$  (squares) and  $\beta = 12/\pi^2$  (triangles) are compared to the full 3D results shown in figure 3 and depicted here by a solid line. The inset gives the relative difference between the 2D Stokes–Darcy model ( $\beta = 1$ , squares, and  $\beta = 12/\pi^2$ , triangles) and the 3D calculations. Note that these data were obtained by the difference between values of accuracy of the order of a few  $10^{-3}$ , which results in the small dispersion observed in the figure.

( $d \rightarrow \infty$ ), which gives

$$f_{SD,\Gamma \rightarrow \infty} \simeq \psi(1 - \psi) - \left( \frac{3}{4} - \psi(1 - \psi) \right) \sqrt{\frac{\beta}{3}} \frac{b}{H} + O\left( \left( \frac{b}{H} \right)^2 \right) \quad (3.5)$$

for the Stokes–Darcy flux and

$$f_{\Gamma,\Gamma \rightarrow \infty} \simeq \psi(1 - \psi) - \left( \frac{3}{4} - \psi(1 - \psi) \right) \frac{186 \text{Zeta}(5)}{\pi^5} \frac{b}{H} + O\left( \left( \frac{b}{H} \right)^2 \right) \quad (3.6)$$

for the full 3D rectangular cell flux (with  $\text{Zeta}(5) = \sum_1^\infty n^{-5} = 1.03693$ , the value of the Riemann-Zeta function). We note that the leading term of both series corresponds to the expected porous media Darcy limit (see (2.12)) with a permeability  $\kappa = b^2/12$ . However, the next-order term ( $O(b/H)$ ) is not the same, unless one chooses for the factor  $\beta$ ,

$$\beta = 3 \left( \frac{186 \text{Zeta}(5)}{\pi^5} \right)^2 \simeq 1.192, \quad (3.7)$$

which is very close to the value  $12/\pi^2 \simeq 1.215$  found by Zeng *et al.* (2003) and to the value  $6/5$  proposed by Ruyer-Quil (2001). The lock-exchange diffusion coefficient has been computed, with the same procedure as above, by integrating (2.9), using  $f_{SD}(\psi)$ , from  $\psi = 0.5$ , and matching the asymptotics  $\zeta = -\zeta_0 + 8d^2\psi^3/(9\zeta_0)$  in the vicinity of the boundary  $\psi = 0$ . The so-obtained lock-exchange diffusion coefficients, calculated for two different values of  $\beta$  ( $\beta = 1$  and  $\beta = 12/\pi^2$ ) are compared with the 3D calculations in figure 4. The data for both values of  $\beta$  are indeed very close to the 3D data over the whole range of aspect ratios,  $\Gamma = 1-100$ . The inset of figure 4 gives the percentage of error for the two values of  $\beta$ . We note that these data were obtained by the difference between values of accuracy of the order of a few  $10^{-3}$ , which results in the small dispersion observed in the inset of figure 4. As expected, the results at large  $\Gamma$  (in the Hele-Shaw regime) are closer to the 3D full problem for  $\beta = 12/\pi^2$

than for  $\beta = 1$ . We point out that, whereas the Brinkman term does bring a significant correction, the exact value of the Brinkman viscosity factor  $\beta$  is however not crucial. For instance, for  $\Gamma = 10$ , we obtained a diffusion coefficient 3.5 % smaller than the 3D value for  $\beta = 1$  and 0.1 % larger for  $\beta = 12/\pi^2$ , to be compared with 30 % of error if the cell was assumed to be of infinite aspect ratio (Hele-Shaw limit), as in Huppert & Woods (1995). In conclusion, we have shown that the 2D Stokes–Darcy model for lock-exchange in a rectangular cell captures quite accurately the effect of the finiteness of the cross-sectional aspect ratio. By using the correct  $\beta$  value, the error in the model is smaller than 5 % for aspect ratios larger than  $\Gamma > 1$ .

#### 4. Experiments

In this section, we present experimental measurements of the diffusion coefficient in Hele-Shaw cells of different aspect ratios and compare them with the computed values.

We used borosilicate rectangular cells of height  $H$  and thickness  $b$  and typical length 30 cm (figure 1). The rectangular cross-sections of the cells were (in mm<sup>2</sup>)  $2 \times 6$ ,  $2 \times 12$ ,  $2 \times 20$ ,  $3 \times 3$ ,  $3 \times 9$ ,  $3 \times 30$ ,  $4 \times 6$ ,  $4 \times 10$  and  $6 \times 6$ . Each cell was used with one side or the other held vertically, leading to two aspect ratios per cell. With such values, we covered a wide range of aspect ratios, from  $\Gamma = H/b = 1/10$  to 10. We used aqueous solutions of natrosol and calcium chlorite as Newtonian miscible fluids. The fluids had equal viscosities, which were fixed by the polymer concentration and measured with an accuracy of 1 %. The fluid densities were adjusted by addition of salt and measured with an accuracy of 0.01 %. The overall accuracy in  $D_{HS}$  was typically 5 %, when taking into account the above accuracies in viscosities and densities and the inherent temperature variations during the experiments. The viscosities and densities of the fluids were chosen to satisfy two experimental requirements. The experiments must be fast enough in order to prevent any significant molecular mixing of the fluids and one should be able to put the two fluids in contact without mixing. The latter condition requires a rather large density contrast and large viscosities. With our cell sizes, a good compromise was obtained with a density contrast of about 1 % and typical viscosities in the range 10–50 mPa s, leading to a lock-exchange diffusion coefficient ranging from  $10^{-3}$  to  $1 \text{ cm}^2 \text{ s}^{-1}$ . The typical Reynolds number built with the gap of the cell of these experiments is smaller than 0.1. For each experiment, the cell was first held with its axis  $Ox$  vertical. The fluids were successively slowly injected, with the lighter fluid on top of the heavier. Thereafter, the cell was closed and put in the desired position, with its axis  $Oz$  vertical in a few seconds. The development of the lock-exchange pseudo-interface was then recorded with a video camera. Typical pictures (side view in the  $z$ – $x$  plane) are given in figure 5 for cells of different aspect ratios. The horizontal axis is scaled with  $\sqrt{D_{HS} t}$ , so that one can see the decrease of  $\zeta_0$  as  $\Gamma$  decreases. With this representation using the self-similar variable  $\zeta = x/\sqrt{D_{HS} t}$ , the profiles are stationary. Note that the trailing edge is fuzzy. This can be attributed to the stick condition at the upper wall. The dark dense fluid stays at the walls for a long time, in particular in the corners of the cross-section. The same phenomenon takes place at the bottom of the cell, but the presence of transparent light fluid has little effect on the turbidity of the heavy dark fluid, and is therefore not noticeable on the pictures. It is worth noting that the shape of the leading edge evolves from an edge at large aspect ratios  $\Gamma$  to a more and more step-like shape as  $\Gamma$  decreases. Note also that for small aspect ratios, although it is rather difficult to take pictures, a top view of the cell reveals a mild spanwise dependency of the interface, but we do not observe the

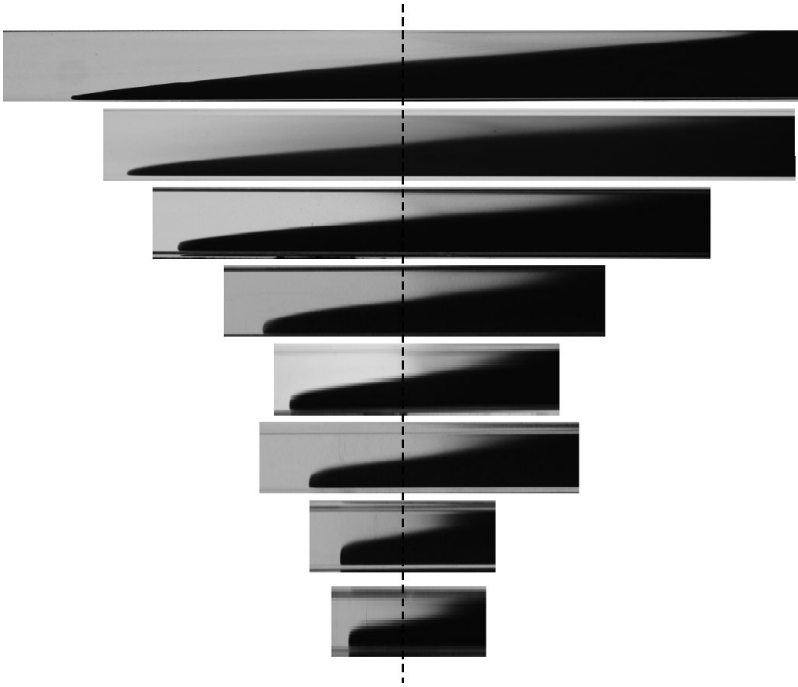


FIGURE 5. Side view (the  $z$ - $x$  plane) of the lock-exchange interface for rectangular cells of aspect ratios  $\Gamma = H/b = 10, 6, 2.5, 1.5, 1, 2/3, 0.4$  and  $1/3$ , from top to bottom, respectively. The horizontal axis is scaled with  $\sqrt{D_{HS} t}$ , which allows one to observe the decrease of  $\zeta_0$  as  $\Gamma$  decreases. The vertical dashed line corresponds to  $\zeta = 0$ .

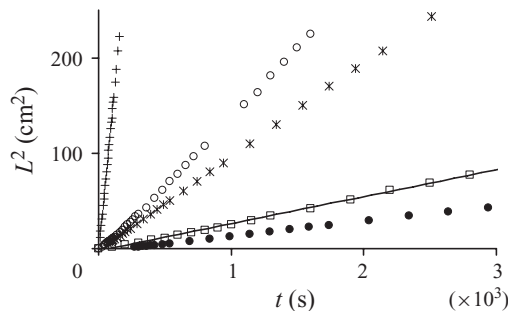


FIGURE 6. Plot of the square of the spreading distance of the leading edge of the front versus time for five cells: Symbols:  $\bullet$ ,  $H = 3$  mm,  $b = 30$  mm;  $\square$ ,  $H = 6$  mm,  $b = 2$  mm;  $*$ ,  $H = 6$  mm,  $b = 4$  mm;  $\circ$ ,  $H = b = 6$  mm;  $+$   $H = 30$  mm,  $b = 3$  mm. The solid line is a linear fit to the data, the slope of which gives the diffusion coefficient plotted in figure 7(a).

spanwise lobe-and-cleft instability reported by Simpson (1972). For each experiment, the locations of the leading and trailing edges of the front were measured in time. Figure 6 gives the variations of the square of the spreading distance versus time for five cells. It is worth noting that the dependency is almost linear, therefore, a linear fit provided the lock-exchange diffusion coefficient, with a typical accuracy of 20%. Figure 7(a) displays the so-obtained normalized lock-exchange diffusion coefficient as a function of  $\Gamma$ . One can see that the agreement with the 3D calculations over the two decades of our measurements is rather good. We note that for the large aspect ratio

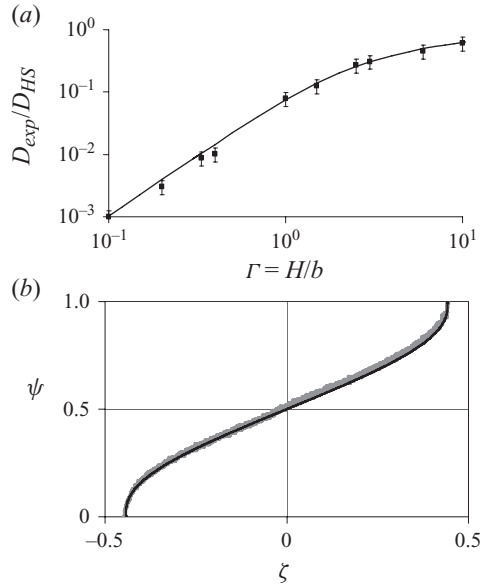


FIGURE 7. (a) Log–log plot of the normalized measured lock-exchange diffusion coefficient,  $D_{exp}/D_{HS}$  (solid squares), versus the aspect ratio,  $\Gamma = H/b$ , of the cell. The solid line corresponds to the 3D results (same as in figure 4). (b) Superimposition of the measured pseudo-interface between the two fluids (grey fuzzy line) and the theoretical profile (full dark line) corresponding to figure 2. The aspect ratio is  $\Gamma = 4$ .

limit of the experiments (up to  $\Gamma = 10$ ), the Hele-Shaw cell limit is not reached, and would underestimate by 30 % the lock-exchange diffusion coefficient. This result thus confirms that for such aspect ratios, one should either compute the full 3D Stokes equation or use the Stokes–Darcy model to obtain the correct behaviour. We also note that our calculation still holds for aspect ratios as small as  $\Gamma = 0.1$ . This result is quite unexpected since for such aspect ratios, some spanwise dependency of the profile was observed, and the hypothesis of the interface surface,  $h(x, y, z)$ , invariant in the  $y$ -direction, is certainly broken. Figure 7(b) displays the superimposition of the theoretical and experimental interfaces between the fluids, for an aspect ratio  $\Gamma = 4$ . The agreement between the two is rather good, thus validating our model. Such an agreement is rather surprising as our small slope assumption is violated at the edges of the gravity current. This agreement, as already emphasized by Huppert (1982) and Séon *et al.* (2007), is likely to be common to viscosity-dominated gravity current without surface tension.

## 5. Conclusion

The viscous lock-exchange diffusion coefficient reflects the competition between the buoyancy-driving effect and the viscous damping, and depends on the geometry of the channel. We give the backbone to calculate this coefficient in different configurations. We recall its computation for a porous medium as already found by Huppert & Woods (1995), and compute it for a 2D Stokes flow between two parallel horizontal boundaries separated by a vertical height,  $H$ . This result is in agreement with E. Hinch (2007, personal communication) and in reasonable agreement with recent

computations by Taghavi *et al.* (2009). Using a quasi-parallel flow assumption, we have calculated the pseudo-interface profile between the two fluids and the diffusion coefficient of viscous lock-exchange gravity currents for a rectangular channel (horizontal thickness  $b$  and vertical height  $H$ ) of any aspect ratio ( $H/b$ ). This analysis provides a crossover between the 2D Stokes flow between two parallel horizontal boundaries separated by a vertical height,  $H$ , and the Hele-Shaw cell limit (applying for  $H/b > 100$ ). Moreover, the shape of the profiles allows us to account for the discrepancy observed at the nose of the gravity current in the experiments by Huppert & Woods (1995). However, the agreement, obtained despite the failure of the lubrication assumption at the edges of the current, should deserve further theoretical investigation. Our calculations of the diffusion coefficient and the shape of the profile have also been convincingly compared with new experiments carried out in cells of various aspect ratios (1/10 to 10). We have also calculated the lock-exchange diffusion coefficient for the same rectangular cells, using the 2D Stokes–Darcy model. This model is shown to apply to aspect ratios  $H/b > 1$ , provided that the appropriate Brinkman correction is used. Such a 2D model may be useful to describe gravity currents with a finite volume of release, with fluids of different viscosities, or in heterogeneous vertical fractures.

D.S. is partially supported by the Institut Universitaire de France. This work was partly supported by CNES (no. 793/CNES/00/8368) and ESA (no. AO-99-083), by Réseaux de Thématiques de Recherches Avancées ‘Triangle de la physique’ and by the Initial Training Network (ITN) ‘Multiflow’ and by French Research National Agency (ANR) through the ‘Captage et Stockage du CO<sub>2</sub>’ programme (project CO-LINER no. ANR-08-PCO2-004-01). All these sources of support are gratefully acknowledged.

## REFERENCES

- BEAR, J. 1988 *Dynamics of Fluids in Porous Media*. Elsevier.
- BENJAMIN, T. J. 1968 Gravity currents and related phenomena. *J. Fluid Mech.* **31**, 209–248.
- BIRMAN, V. K., MARTIN, J. E. & MEIBURG, E. 2005 The non-Boussinesq lock-exchange problem. Part 2. High-resolution simulations. *J. Fluid Mech.* **537**, 125–144.
- BIZON, C., WERNE, J., PREDTECHENSKY, A., JULIEN, K., MCCORMICK, W., SWIFT, J. & SWINNEY, H. 1997 Plume dynamics in quasi-2D turbulent convection. *Chaos* **7**, 107–124.
- BONOMETTI, T., BALACHANDAR, S. & MAGNAUDET, J. 2008 Wall effects in non-Boussinesq density currents. *J. Fluid Mech.* **616**, 445–475.
- BRINKMAN, H. 1947 A calculation of the viscous forces exerted by a flowing fluid on a dense swarm of particles. *Appl. Sci. Res.* **A1**, 27–39.
- CANTERO, M., LEE, J., BALACHANDAR, S. & GARCIA, M. 2007 On the front velocity of gravity currents. *J. Fluid Mech.* **586**, 1–39.
- DIDDEN, N. & MAXWORTHY, T. 1982 The viscous spreading of plane and axisymmetric gravity currents. *J. Fluid Mech.* **121**, 27–42.
- FERNANDEZ, J., KUROWSKI, P., PETITJEANS, P. & MEIBURG, E. 2002 Density-driven unstable flows of miscible fluids in a Hele-Shaw cell. *J. Fluid Mech.* **451**, 239–260.
- GONDRET, P., RAKOTOMALALA, N., RABAUD, M., SALIN, D. & WATZKY, P. 1997 Viscous parallel flows in finite aspect ratio Hele-Shaw cell: analytical and numerical results. *Phys. Fluids* **9**, 1841–1843.
- GRAF, F., MEIBURG, E. & HÄRTEL, C. 2002 Density-driven instabilities of miscible fluids in a Hele-Shaw cell: linear stability analysis of the three-dimensional Stokes equations. *J. Fluid Mech.* **451**, 261–282.
- GRATTON, J. & MINOTTI, F. 1990 Self-similar viscous gravity currents: phase-plane formalism. *J. Fluid Mech.* **210**, 155–182.

- HALLEZ, Y. & MAGNAUDET, J. 2009 A numerical investigation of horizontal viscous gravity currents. *J. Fluid Mech.* **630**, 71–91.
- HUPPERT, H. H. 1982 The propagation of two-dimensional and axisymmetric viscous gravity currents over a rigid horizontal surface. *J. Fluid Mech.* **121**, 43–58.
- HUPPERT, H. H. & WOODS, A. W. 1995 Gravity-driven flows in porous layers. *J. Fluid Mech.* **292**, 55–69.
- LOWE, R. J., ROTTMAN, J. W. & LINDEN, P. F. 2005 The non-Boussinesq lock-exchange problem. Part 1. Theory and experiments. *J. Fluid Mech.* **537**, 101–124.
- MARTIN, J., RAKOTOMALALA, N. & SALIN, D. 2002a Gravitational instability of miscible fluids in a Hele-Shaw cell. *Phys. Fluids* **14**, 902–905.
- MARTIN, J., RAKOTOMALALA, N., SALIN, D. & BÖCKMANN, M. 2002b Buoyancy-driven instability of an autocatalytic reaction front in a Hele-Shaw cell. *Phys. Rev. E* **65**, 051605.
- NEUFELD, J. A. & HUPPERT, H. E. 2009 Modelling carbon dioxide sequestration in layered strata. *J. Fluid Mech.* **625**, 353–370.
- RUYER-QUIL, C. 2001 Inertial corrections to the Darcy law in a Hele-Shaw cell. *C. R. Acad. Sci. Paris* **329**, Serie IIb 337–342.
- SÉON, T., ZNAÏEN, J., SALIN, D., HULIN, J. P., HINCH, E. J. & PERRIN, B. 2007 Transient buoyancy-driven front dynamics in nearly horizontal tubes. *Phys. Fluids* **19**, 123603.
- SHIN, J. O., DALZIEL, S. B. & LINDEN, P. F. 2004 Gravity currents produced by lock exchange. *J. Fluid Mech.* **521**, 1–34.
- SIMPSON, J. E. 1972 Effects of the lower boundary on the head of a gravity current. *J. Fluid Mech.* **53**, 759–768.
- TAGHAVI, S. M., SEON, T., MARTINEZ, D. M. & FRIGAARD, I. A. 2009 Buoyancy-dominated displacement flows in near-horizontal channels: the viscous limit. *J. Fluid Mech.* **639**, 1–35.
- TAKAGI, D. & HUPPERT, H. 2007 The effect of confining boundaries on viscous gravity currents. *J. Fluid Mech.* **577**, 495–505.
- TALON, L., MARTIN, J., RAKOTOMALALA, N., SALIN, D. & YORTSOS, Y. 2003 Lattice BGK simulations of macrodispersion in heterogeneous porous media. *Water Resour. Res.* **39**, 1135–1142.
- ZENG, J., YORTSOS, Y. C. & SALIN, D. 2003 On the Brinkman correction in unidirectional Hele-Shaw flows. *Phys. Fluids* **15**, 3829–3836.